

VIP Very Important Paper



Broadband-Emitting 2D Hybrid Organic–Inorganic Perovskite Based on Cyclohexane-bis(methylammonium) Cation

Ishita Neogi⁺,^[a] Annalisa Bruno⁺,^{*[a, b]} Damodaran Bahulayan,^[a] Teck Wee Goh,^[b] Biplab Ghosh,^[a, c] Rakesh Ganguly,^[b] Daniele Cortecchia,^[a, b, c] Tze Chien Sum,^[b] Cesare Soci,^[b] Nripan Mathews,^{*[a, d]} and Subodh Gautam Mhaisalkar^{*[a, d]}

A new broadband-emitting 2D hybrid organic–inorganic perovskite (CyBMA)PbBr₄ based on highly flexible *cis*-1,3-bis(methylamino)hydrobromide)cyclohexane (CyBMABr) core has been designed, synthesized, and investigated, highlighting the effects of stereoisomerism of the templating cation on the formation and properties of the resulting perovskite. The new 2D material has high exciton binding energy of 340 meV and a broad emission spanning from 380 to 750 nm, incorporating a prominent excitonic band and a less intense broad peak at room temperature. Significant changes in the photolumines-

cence (PL) spectrum were observed at lower temperatures, showing remarkable enhancement in the intensity of the broadband at the cost of excitonic emission. Temperature-dependent PL mapping indicates the effective role of only a narrow band of excitonic absorption in the generation of the active channel for emission. Based on the evidences obtained from the photophysical investigations, we attributed the evolution of the broad B-band of (CyBMA)PbBr₄ to excitonic self-trapped states.

Introduction

Hybrid organic–inorganic perovskites (HOIPs) semiconductors have attracted significant attentions owing to their outstanding performance in photovoltaics.^[1] The high efficiency ach-

ieved along with their appealing low-cost solution processability, led to the development of Pb-based HOIPs as substitute for silicon-based solar cell technology.^[2] In general, HOIPs display diverse dimensionality owing to the templating action of the inorganic metal-halide lattice. When the metal-halide network extends in 3D space incorporating small organic ammonium cations in the cuboctahedral voids, the generated lattice is recognized as 3D HOIPs, symbolized as AMX₃, where A and M are monovalent and divalent cations, respectively.^[3]

However, if the metal-halide sheets are separated by relatively bigger organic ligands, represented as (RNH₃)₂PbX₄ or (NH₃RNH₃)PbX₄, the obtained lamellar type architectures have reduced dimensionality, and are termed 2D or layered HOIPs.^[3] Such low dimensional systems allow a greater synthetic flexibility and a consequent fine tuning of the materials properties through synthetic design. In general, the ligands of 2D HOIPs are bulky as well as hydrophobic in nature, which manifests in their ambient moisture resistance, substantially lacking in the corresponding 3D materials. Moreover, 2D HOIPs display significantly higher exciton binding energy compared to the analogous 3D materials owing to their multi-quantum-well-like architecture.^[3] All these unprecedented features of 2D HOIPs have paved the way for their emergence as extremely desirable materials for various light-emission applications, such as light-emitting devices (LEDs)^[4] lasing,^[5] photodetectors,^[6] and scintillation.^[7]

In the current decade, when paradigms have shifted toward the development of sustainable technologies to retrench energy consumptions, phosphor-based solid-state lighting

[a] Dr. I. Neogi,⁺ Dr. A. Bruno,⁺ Dr. D. Bahulayan, B. Ghosh, D. Cortecchia, Prof. N. Mathews, Prof. S. G. Mhaisalkar
Energy Research Institute, Nanyang Technological University
Research Techno Plaza, X-Frontier Block, Level 5
50 Nanyang Drive, 637553 Singapore (Singapore)
E-mail: nripan@ntu.edu.sg
subodh@ntu.edu.sg

[b] Dr. A. Bruno,⁺ T. W. Goh, Dr. R. Ganguly, D. Cortecchia, Prof. T. C. Sum, Prof. C. Soci
School of Physical and Mathematical Science
Nanyang Technological University
21 Nanyang Link, 637371 Singapore (Singapore)
E-mail: annalisa@ntu.edu.sg

[c] B. Ghosh, D. Cortecchia
Interdisciplinary Graduate School
Nanyang Technological University
50 Nanyang Avenue, 639798 Singapore (Singapore)

[d] Prof. N. Mathews, Prof. S. G. Mhaisalkar
School of Materials Science and Engineering
Nanyang Technological University
Nanyang Avenue, 639798 Singapore (Singapore)

[*] These authors contributed equally to this work.

Supporting Information for this article can be found under <https://doi.org/10.1002/cssc.201701227>.

This publication is part of dual Special Issues on Perovskite Optoelectronics published in *ChemSusChem* and *Energy Technology*. Please visit the *ChemSusChem* issue at <http://doi.org/10.1002/cssc.v10.19>, and the companion issue of *Energy Technology* at <http://dx.doi.org/10.1002/ente.v5.10>.

evolved as potential substitute for conventional incandescent bulbs. In general, the majority of 3D HOIPs have sharp and narrow band-edge-to-band-edge emission. However, the same is not the case with 2D HOIPs, which can substantially achieve broad emission. These broadband-emitting 2D HOIPs are envisaged to have potentials for low-cost, single source, solution-processed, solid-state lighting, and are anticipated to be potential substitutes for contemporary multi-phosphor-based white-light emission technology, in which significant energy loss due to self-absorption by phosphor is a major setback.^[8] Insofar, a number of low-dimensional HOIPs have shown broadband emission based on both linear and cyclic organic cations to template the 2D perovskite structure. These include for example: 3-(aminopropyl)imidazole,^[9] *N*1-methylethane-1,2-diammonium(*N*-MEDA),^[10] 2,2'(ethylenedioxy)bis(ethylammonium) (EDBE)^[11] and cyclohexyl ammonium cation.^[13a] Recently, white-light emission has been also shown in 1D structures employing *N,N'*-dimethylethylenediamine as organic building block.^[12] It should be noted that broadband emission of the above described 2D HOIPs involves various mechanisms, including emission either from the defect states, trap states, or energy transfer.^[9–11,13] Recently, the origin of white-light emission in 2D perovskites has been reported to be related to the charge self-trapping phenomena leading to the formation of polaronic excitons localized within the inorganic layers of the perovskite.^[13a,b,14] Such charge self-trapping was shown to be energetically favored in low-dimensional perovskites bearing strong excitonic properties and subject to strong distortion of the lead-halide framework.^[10,14] These findings point to the need of designing perovskites with distorted and strained structures to enhance charge self-trapping that may ultimately lead to highly efficient broadband emission.

In continuation of our strategies to develop functional perovskite materials,^[13a,14,15] we designed and explored a new white-light emitting 2D HOIP embodying 1,3-bis(methylamino)hydrobromide)cyclohexane(CyBMABr) ligand (Figure 1). Our choice for exploring CyBMABr as ligand for 2D HOIP was moti-

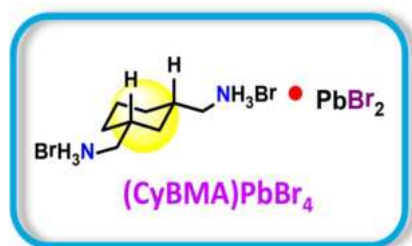


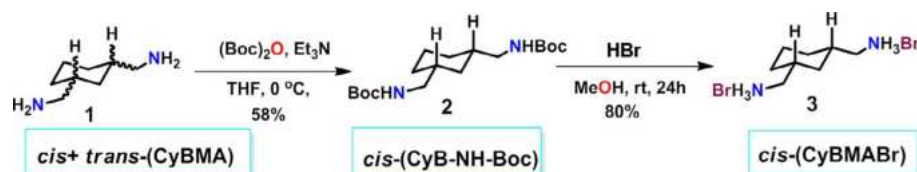
Figure 1. Structure of (CyBMA)PbBr₄.

vated on the following grounds: we envisioned that bidentate ligand CyBMABr will bring the layers of [PbBr₆]⁴⁻ octahedra nearer compared to the other monodentate ligands. Furthermore, the angular orientation of the methylammonium moieties involved in hydrogen bonding with the inorganic scaffold, combined with the steric hindrance induced by the cyclohexyl core, would induce structural distortions in the perovskites lattice. In particular, the conformational isomerism of CyBMABr may enhance cumulative lattice vibrations and charge-phonon coupling in the corresponding perovskite.^[13b,c,17] Although a few white-light emitting perovskites have recently been reported, the effects of stereoisomerism imparted by the templating cation on the formation and properties of the resulting perovskite have never been investigated. Herein, we isolated both *cis* and *trans* diastereomers of the ligand CyBMABr and observed that the steric hindrance, particularly 1,3-diaxial interaction between the methylammonium group and 1,3-axial hydrogens of the *trans* isomer of the ligand hinders the crystallization of the perovskite. On the other hand, the *cis* diastereomer can be successfully cocrystallized with the inorganic precursor leading to the formation of the 2D HOIP, namely, *cis*-(CyBMA)PbBr₄ (Figure 1). We inferred that the angular tension induced by the *cis* ligand on the inorganic lattice causes wide emission in the visible region. The synthesis, crystal structure, and broadband-emissive properties of (*cis*-CyBMA)PbBr₄ are discussed.

Results and Discussion

Synthesis

The reaction scheme for the isolation of [*cis*-(CyBMABr)] from *cis* + *trans*(CyBMA) (**1**) is reported in Scheme 1. The diamine (CyBMA) was reacted with di-*tert*-butyldicarbonate to form the corresponding Boc-protected amine, CyB-NH-Boc (Boc: *tert*-butoxycarbonyl). Washing of the latter with hexane/THF (1:1) led to the isolation of **2**, as white powder with 58% yield. The *cis* conformation of **2** was established from the crystal structure analysis reported in Figure S11 in the Supporting Information. Subsequent deprotection of **2** with 48% aqueous HBr at room temperature led to the formation of corresponding ammonium bromide (**3**). To synthesize the corresponding perovskite crystals, equimolar ratio (0.27 millimoles) of **3** and PbBr₂ were mixed with 5 mL (48%) aqueous HBr, and sonicated for 5 min to completely dissolve them. (CyBMA)PbBr₄ perovskite single crystals were grown by slow diffusion of dioxane over a period of a month. The isolated *trans*-(CyB-NH-Boc) was also treated with HBr to synthesize corresponding *trans*-(CyBMABr). The synthesis process for *trans*-(CyB-NH-Boc) and *trans*-(CyBMABr)



Scheme 1. Synthesis of *cis*-CyBMABr.

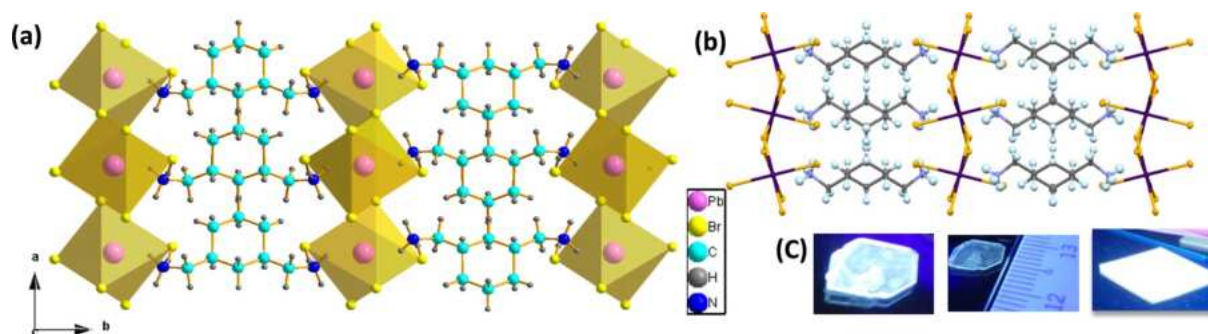


Figure 2. (a) Crystal packing diagram for (CyBMA)PbBr₄ showing propagation of [PbBr₆]⁴⁻ octahedron along the *ac*-plane, (b) packing along the *bc*-plane revealing twist of the Pb–Br chains, (c) photographs of a (CyBMA)PbBr₄ crystal with scale bar and spin-coated film illuminated under UV lamp.

are described in the experimental section and the ¹H and ¹³C NMR data are shown in Figures S1–S10. However, *trans*-(CyBMA)Br did not allow the perovskite formation when cocrystallized with PbBr₂ in HBr solution.

Crystal structure, morphology, and thermal stability

(CyBMA)PbBr₄ crystals (Figures 2 and S11) were characterized by XRD at various temperatures and the structural parameters remained unchanged in the temperature range investigated (298–403 K, Table S2). (CyBMA)PbBr₄ was found to crystallize into orthorhombic crystal system (*Pnma*) with <100> orientation, Table 1. The [PbBr₆]⁴⁻ octahedron propagates in *ac*-plane with channels along the *b*-axis occupied with the ligand molecules (Figure 2). The asymmetric unit includes half molecule of the ligand, one Pb²⁺, and two bromide ions. The propagating Pb–Br chains are twisted such that plane passing through each axial Pb–Br bond in the *bc*-plane is slanted by 28° with respect to the plane of the axial Pb–Br bond of the adjacent octahedra within the same chain (cf. Figure 2b). As a result, the Pb–Br–Pb bond angles, which drive the connectivity of the inorganic motif, strongly deviate from the planar geometry

with an average value of 147.72°. Despite the relevant tilt, we note that the PbBr₆ units maintain a close to ideal geometry of the octahedral coordination with an octahedral elongation of $\lambda_{\text{oct}} = 1.0016$ and octahedral angle variance $\sigma_{\text{oct}}^2 = 5.98$. The reason for such twist, leading to a strong deviation from the ideal planar structure, relates to the hydrogen bonding between the methyl ammonium groups of the ligands and the Pb–Br octahedra, generating the <100>-oriented inorganic network with highly twisted PbBr₆ octahedral units. The interplanar distance between the adjacent Pb–Br chains of (CyBMA)PbBr₄ was approximately 12 Å, which is consistent with the short length of our templating cation. Furthermore, the cyclohexane ring of the ligand *cis*-CyBMA)Br exists in its most stable chair conformation and the angle between methyl ammonium group and cyclohexane core is about 110°. The torsional angle between the two 1,3-methyl ammonium linkers is approximately 0° due to their equatorial position. The preferred orientation along the *b*-axis was revealed from prominent XRD reflections of the film of (CyBMA)PbBr₄ (Figure S13).

Images of the 2D platelets of (CyBMA)PbBr₄ and the corresponding thin films under UV-light illumination show bright white-light emission (Figure 2c). To test the thermal stability of the material, thermogravimetric analysis (TGA) was performed on the isolated crystals of (CyBMA)PbBr₄ and is shown in Figure S14. The onset of decomposition was detected at 319 °C, which attests to the high thermal stability of (CyBMA)PbBr₄. The TGA curve displays two weight-loss steps; the first can be attributed to the loss of organic cation and the second to the decomposition of the inorganic residue.

Photophysical properties

(CyBMA)PbBr₄ thin films were prepared following the procedure described in the Experimental Section. A scanning electron microscopy (SEM) image of the thin film demonstrating its uniform and smooth morphology is shown in Figure S15. The UV/Vis spectrum for the (CyBMA)PbBr₄ thin film measured at 298 K is shown in Figure 3. It shows a broad UV absorption spanning over the range 300–350 nm and a sharp peak at 380 nm. The excitonic absorption peak is typical of layered perovskites owing to the quantum confinement between the organic barrier and the inorganic wells. The energy difference between the valence and excitonic band is approximately

Table 1. XRD data of (CyBMA)PbBr ₄ .	
Structural parameters	(CyBMA)PbBr ₄
molecular formula	C ₁₈ H ₃₄ N ₂ O ₄
formula weight	671.09
crystal system	orthorhombic
space group	<i>Pnma</i>
<i>a</i> [Å]	8.513(6)
<i>b</i> [Å]	24.424(16)
<i>c</i> [Å]	7.9371(6)
α (°)	90
β (°)	90
γ (°)	90
volume (Å ³)	1650.3(2)
calculated density [mg m ⁻³]	2.701
absorption coefficient [mm ⁻¹]	19.885
<i>F</i> (000)	1216
goodness-of-fit on <i>F</i> ²	1.035
final <i>R</i> indices [<i>I</i> > 2 σ (<i>I</i>)]	<i>R</i> 1 = 0.0904, <i>wR</i> 2 = 0.2502 ^[a]
<i>R</i> indices (all data)	<i>R</i> 1 = 0.1306, <i>wR</i> 2 = 0.2881 ^[a]

[a] *R*1 and *wR*2 are a measure of the agreement between the crystallographic model and the experimental X-ray diffraction data.

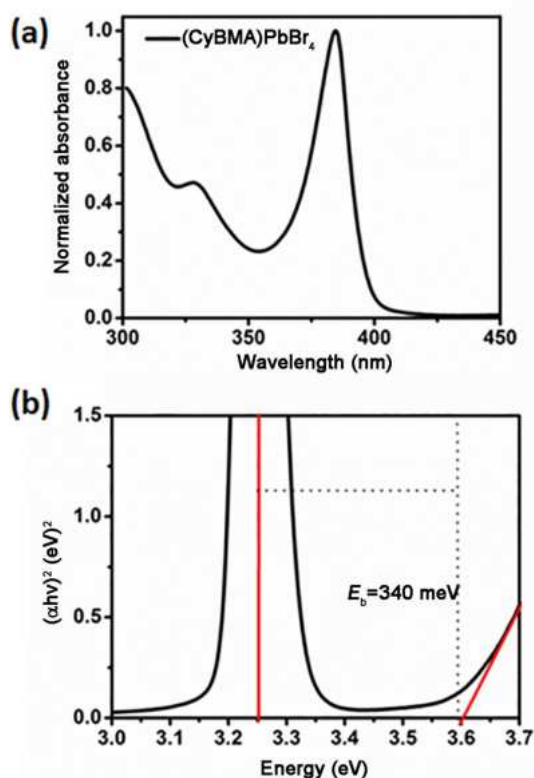


Figure 3. (a) UV/Vis absorption spectrum at 298 K, (b) Tauc plot at 77 K. The exciton binding energy of (CyBMA)PbBr₄ was extracted as the difference between the center of the excitonic band and the inception of the higher-energy band.

3.65 eV, calculated from Tauc plot for direct band-gap semiconductor material, where $\alpha \propto (E - E_g)^{1/2}$ (Figure S16).^[18] Furthermore, to evaluate the exciton binding energy of the material, temperature-dependent UV/Vis studies were performed for the (CyBMA)PbBr₄ thin film in the temperature range from 298 to 77 K (Figures 3a–b and S17). We observed a slight blue shift and narrowing of the absorption band edge with lowering of temperature, in agreement with previous results.^[18b,c] The exciton binding energy was measured from the UV/Vis spectrum

of (CyBMA)PbBr₄ at 77 K, by subtracting the onset of interband transition from the excitonic emission peak (Figure 3b).

The high exciton binding energy of 340 meV for (CyBMA)PbBr₄ is in agreement with its low dimensionality. The photoluminescence (PL) spectrum of the (CyBMA)PbBr₄ spin-coated film, excited at 360 nm, exhibits two main components: a sharp and dominant excitonic peak with maximum at 400 nm (E-band), and a less intense broader band (B-band) spanning over the visible range between 450 and 750 nm (Figure 4a). The dominant excitonic peak is a typical feature of 2D HOIP with non-luminescent chromophore. Emission characteristics of (CyBMA)PbBr₄ were explored as a function of temperature to probe the nature of emissive states. Interestingly, upon lowering the temperature, the (CyBMA)PbBr₄ PL emission spectrum showed disappearance of the E-band with simultaneous enhancement of the B-band (Figure 4a,b). The Commission Internationale de L'Éclairage (CIE) chromaticity coordinates for the emission of (CyBMA)PbBr₄ at 298 K are: $x=0.23$ and $y=0.29$, which occupies the bluish-white region of the coordinate diagram. We noted that the relative changes in the intensity of both E- and B-band with temperature drift the emission from blue to red, as shown in Figure 4c. The correlated color temperature (CCT) coordinates at 298 and 77 K were 18418 and 3315 K, respectively, conforming the consistent shift to warmer colors. Figure 4b also shows that the total emission intensity strongly increases decreasing the temperature, suggesting that at room temperature a strong thermal quenching of PL takes place, justifying the low photoluminescence quantum efficiency (PLQE) of the material, as reported in Table 2. To tune the emission of the CyBMA-based perovskites close to white, we also explored the mixed-halide compositions by partially exchanging the bromine and iodine atoms content (Figure S19).

Table 2. Photophysical properties of (CyBMA)PbBr ₄			
Material	Band gap [eV]	Binding energy [meV]	PLQE ^[a] [%]
(CyBMA)PbBr ₄	3.65	340	1.5
[a] At 298 K			

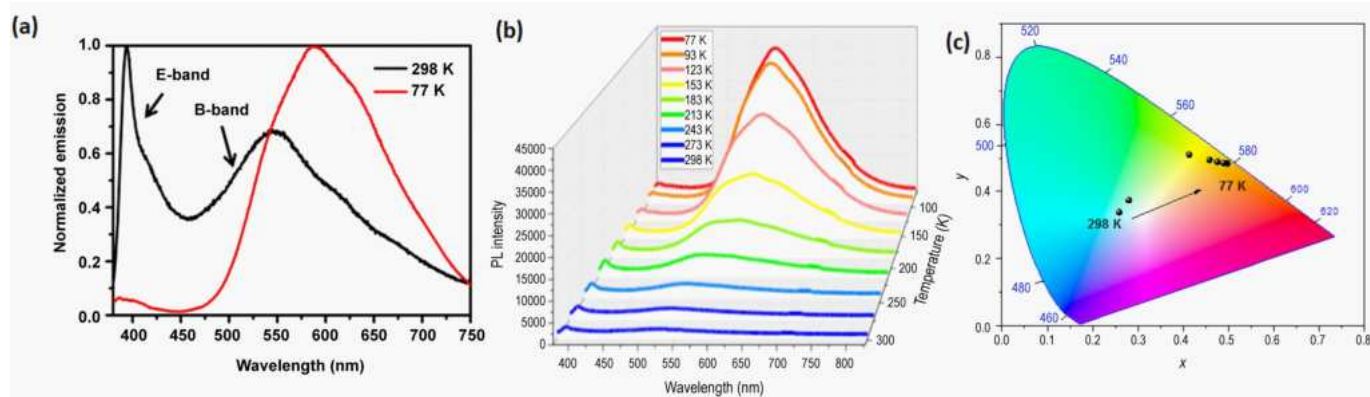


Figure 4. (a) PL spectrum of (CyBMA)PbBr₄ spin-coated film at 298 and 77 K, for 360 nm excitation, (b) temperature-dependent 2D PL map in the range of 298–77 K for excitation at 360 nm, (c) 1931 chromaticity coordinates as a function of temperature.

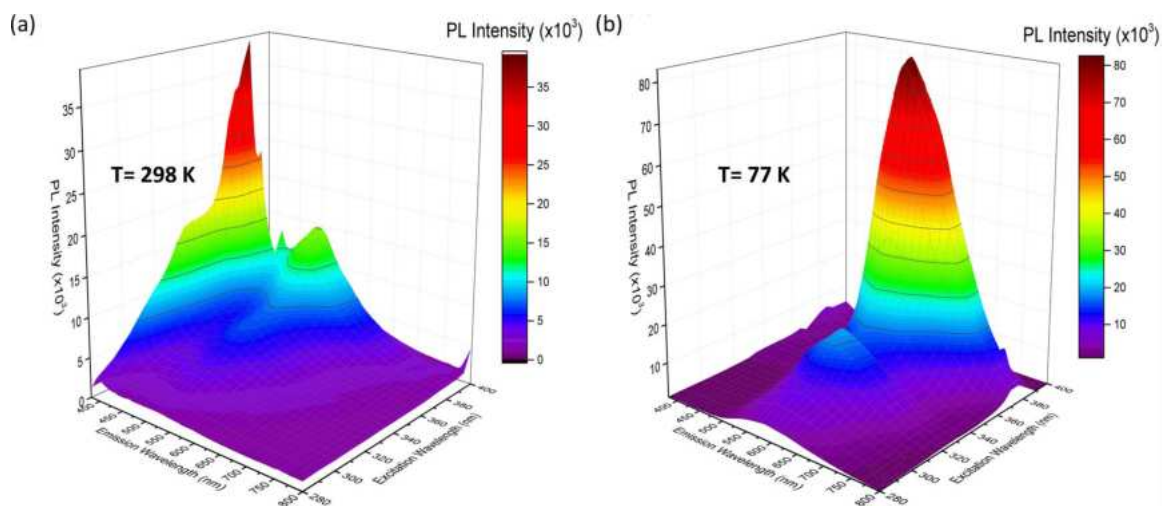


Figure 5. (CyBMA)PbBr₄ PL photoexcitation maps. PL intensity is reported as function of emission and excitation wavelengths at (a) 298 K, and (b) 77 K.

The composition with emission closest to the white point was achieved for the 9:1 bromine/iodine ratio. The corresponding CIE coordinates are $x=0.25$, $y=0.30$.

PL photoexcitation maps at 298 and 77 K are shown in Figure 5a,b, respectively. Interestingly, the (CyBMA)PbBr₄ emission spectrum is very different at 298 and 77 K, although both photoexcitation maps clearly exhibit the same maximum at 360–380 nm (Figure 5), which is in contrast to the broad absorption shown in Figure 3a. Similar behavior has been observed previously in 2D HOIP and attributed to the presence of single active excitation channel that eventually relaxes into the intermediate states, generating broad PL.^[13]

The most accredited model, which explains the nature of the broad PL involves the self-trapping of excitons (STEs),^[19] which is favored in perovskites with strong distortions of the inorganic lattice.^[14,20,21] In the case under study, despite the close-to-ideal geometry of the PbBr₆ units, their strong out-of-plane tilt strongly affects the geometry of the lead-bromide network. Therefore, the interplay between such structural properties in (CyBMA)PbBr₄ well correlates with the coexistence of narrowband and broadband emission with comparable intensity at room temperature. Our temperature-dependent investigation is also in agreement with the proposition that the broad emission of (CyBMA)PbBr₄ could be owed to STEs.^[19] As noted earlier, photoexcitation of (CyBMA)PbBr₄ operates with single active channel, forming bound electron–hole pairs, termed as excitons or free excitons (FEs), which can couple with the inorganic lattice vibrations, that is, phonons, forming coupled exciton–phonon pairs. To simplify the concept, exciton–phonon coupling can be visualized as an exciton dressed with phonons.^[19,22] The greater the extent of exciton–phonon interaction, the slower is the movement of exciton due to association with a higher density of phonons, and for a sufficiently strong exciton–phonon interaction, the movement of exciton is interrupted at a lattice site, leading to their self-trapping. The emission from STEs is very broad and significantly stoke-shifted compared to the excitonic emission, owing to the reorganization of potential during the trapping mecha-

nism. Furthermore, at room temperature, the coexistence of FEs and STEs is well established in several materials with higher dimensionality.^[22b] At room temperature, fast thermal funneling of the generated STEs back to the FEs occurs, which eventually decays to give dominating excitonic emission at room temperature.^[23] This concept can be visualized as temperature-assisted detrapping of STEs. At 77 K, all excitons are in self-trapped states, resulting in a broadband luminescence that is strongly stoke-shifted, as discussed in previous papers.^[12–13c] However, the transformation of STEs to FEs becomes thermodynamically unfavorable at lower temperatures, resulting in quenching of the emission from excitonic state and increasing the population of STEs, which becomes the dominating decay channel.

STEs are generally localized within the inorganic lattice and both experimental electron-spin resonance measurements and ab initio calculations have shown that Pb₂³⁺, Pb³⁺, and X₂[−] (X = Cl, Br) are the most likely radiative self-trapped states.^[18–20]

To further validate the attribution of exciton self-trapping within the (CyBMA)PbBr₄ lattice, room-temperature time-resolved PL (TRPL) was measured for different emission wavelengths from 385 to 605 nm, as shown in Figure 6. Clearly, the characteristic decay time increases as a function of emission wavelength (Figure 6b). These outcomes likewise complement our argument of photogeneration of FEs by single active channel, followed by relaxation into different STEs, causing prompt onset and shorter lifetime compared to that of the red-edge of the emission, similar to the observations reported for *N*-MEDA and Si-nanocrystals and other 2D HOIPs.^[24]

Conclusions

A new 2D hybrid organic–inorganic perovskite, namely, (CyBMA)PbBr₄, was developed with broadband emission in the range 380–750 nm (Commission Internationale de L'Eclairage, CIE, coordinates $x=0.23$ and $y=0.29$) at 298 K. The ligand of (CyBMA)PbBr₄ is endowed with softness and flexibility that can initiate a variety of phonon interactions and further induce a

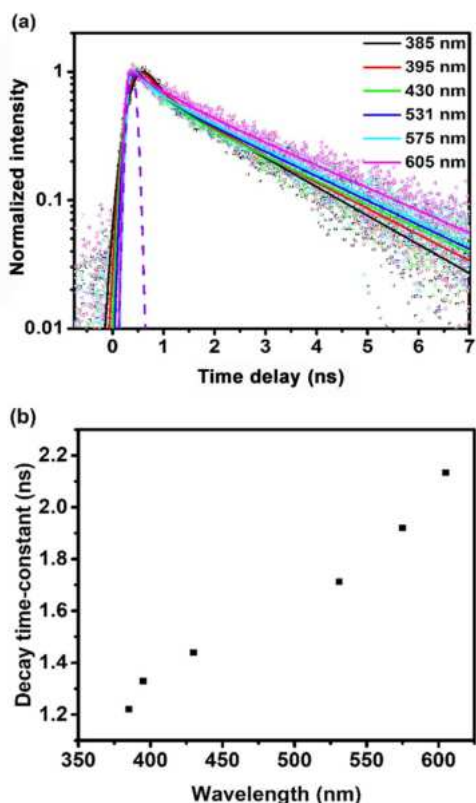


Figure 6. (a) (CyBMA)PbBr₄ time-resolved PL decays. Excitation wavelength is 340 nm at 50 $\mu\text{J cm}^{-2}$ fluence and the emission was collected for different emission wavelengths at 298 K. The data were fitted with a stretched exponential equation: $I(t) = I_0 \times \exp[-(t/\tau)^\beta]$, τ is the characteristic decay time and β is stretching exponent. (b) Decay-times vs. emission wavelengths.

strong twist of the PbBr₆ octahedral units and deviation of the Pb–Br–Pb bond angles from the ideal planar geometry. Thermogravimetric analysis reflected very high thermal stability ($T_g = 319^\circ\text{C}$) of the material. The material possesses a very high binding energy of 340 meV. (CyBMA)PbBr₄ photoluminescence at 298 K was dominated by a sharp excitonic peak (E-band) at 400 nm and a lesser intense broad side band (B-band). Temperature-dependent measurements revealed decay in the intensity of the E-band with simultaneous gain of B-band at lower temperatures. Photoexcitation mappings at 298 and 77 K revealed the contribution of a narrow range of excitonic absorption responsible for photoexcitation of the material, vindicating the presence of a single active channel. The broad emission has been attributed to self-trapped states of various trapping depths. We compellingly propose that the flexibility and softness of the cyclohexane core of CyBMABr can initiate strong exciton–phonon interactions, leading to trapping of excitons inside the self-created potential barriers. Furthermore, we propose that the deformations of the (CyBMA)PbBr₄ inorganic lattice can favor self-trapping by acting as potential sites for self-localization. Finally, (CyBMA)PbBr₄ embodies potentials of a promising phosphor material.

Experimental Section

Materials

1,3-Cyclohexanebis(methylamine) (CyBMA) was purchased from Aldrich in the form of a 3:1 mixture of *cis* and *trans*-diastereomers.

Synthesis of *cis*-(CyB-NH-Boc)

For the isolation and synthesis of *cis*-NH-Boc protected amine from (*cis,trans*)-1,3-cyclohexanebis(methylamine), di-*tert*-butyl dicarbonate (1.6 mL, 7.0 mmol) was slowly added to an ice-cold solution of 1,3-cyclohexanebis(methylamine) (0.5 g, 3.5 mmol) and trimethylamine (1 mL, 7.0 mmol) in Tetrahydrofuran (THF, 15 mL). The reaction mixture was stirred overnight at room temperature. THF was then evaporated, followed by washing of the solid residue with a THF/hexane mixture (1:1), which led to the isolation of *cis*-(CyB-NH-Boc) as a white powder (0.70 g, 58% overall yield); NMR spectra are reported in Figures S1 and S2. Here, we report the main data. ¹H NMR (CDCl₃, 400 MHz) $\delta = 0.06$ (s, 2H), 0.52–0.61 (m, 1H), 0.77–0.87 (m, 2H), 1.18–1.29 (m, 1H), 1.43 (s, 18H), 1.79–1.63 (m, 4H), 2.97 (brs, 4H), 4.58 ppm (brs, NH); ¹³C NMR(CDCl₃, 100 MHz) $\delta = 25.2, 28.4, 30.49, 34.7, 38.0, 46.8, 78.9, 156.0$ ppm.

Synthesis of *cis*-(CyBMABr)

To synthesize *cis*-(CyBMABr), *cis*-(CyB-NH-Boc) (0.1 mg, 0.29 mmol) was dissolved in methanol (5 mL) and was reacted with excess of ($\approx 48\%$) aqueous HBr (0.5 mL). The reaction mixture was stirred overnight at RT. The solvent was removed under vacuum and the residue obtained was washed several times with diethyl ether to obtain the corresponding pure *cis*-ammonium bromide (0.71 mg, 80% overall yield).

Cis-(CyBMABr) NMR spectra are reported in Figures S3 and S4. ¹H NMR (CDCl₃, 400 MHz) $\delta = 0.61$ –0.71 (m, 1H), 0.77–0.87 (m, 2H), 1.11–1.21 (m, 1H), 1.56–1.66 (m, 2H), 1.73–1.80 (m, 4H), 2.58–2.71 (m, 4H), 7.07 ppm (brs, NH); ¹³C NMR(CDCl₃, 100 MHz) $\delta = 24.7, 29.6, 34.0, 35.4, 44.8$ ppm.

Synthesis of *trans*-(CyB-NH-Boc)

For the isolation of *trans*-(CyB-NH-Boc), the washing of *cis*-(CyB-NH-Boc) was left for slow evaporation; this led to crystallization of *cis*- and *trans*-diastereomers in separate forms. *cis*-(CyB-NH-Boc) crystallized as needles and its structure was confirmed by NMR spectroscopy and single-crystal XRD. However, the *trans*-diastereomer was isolated as fan-shaped crystals. Both diastereomers were separated manually.

Trans-(CyB-NH-Boc) NMR spectra are reported in Figures S5 and S6. ¹H NMR (CDCl₃, 400 MHz) $\delta = 1.21$ –1.271 (m, 2H), 1.37–1.38 (m, 2H), 1.46–1.49 (m, 1H), 1.43 (s, 18H), 1.55–1.58 (m, 3H), 1.75 (brm, 2H), 3.13–2.96 (m, 4H), 4.58 ppm (brs, NH); ¹³C NMR(CDCl₃, 100 MHz) $\delta = 20.8, 25.2, 27.4, 28.4, 29.4, 30.5, 31.9, 33.3, 44.6, 78.9, 156.2$ ppm.

Synthesis of *trans*-(CyBMABr)

For the synthesis of *trans*-(CyBMABr), a similar synthetic protocol as the one used for the synthesis of *cis*-(CyB-NH-Boc) was followed. We also compared the ¹H and ¹³C NMR spectra of *cis*-(CyBMABr), *trans*-(CyBMABr), and *cis,trans*-(CyBMABr) (synthesized from dia-

steromeric mixture). *Trans*-(CyBMABr) NMR spectra are reported in Figures S7 and S8.

^1H NMR (CDCl_3 , 400 MHz) $\delta = 1.23\text{--}1.30$ (m, 2H), 1.40–1.45 (m, 4H), 1.50–1.57 (m, 2H), 1.85–1.88 (m, 2H), 2.73 (brs, 4H), 7.73 (brs, NH), 7.07 ppm (brs, NH); ^{13}C NMR (CDCl_3 , 100 MHz) $\delta = 20.0$, 28.2, 30.8, 31.5, 42.6 ppm. ^1H and ^{13}C NMR are summarized in Figures S9 to S10.

Film preparation of (CyBMA)PbBr₄

2D platelets were washed thoroughly with diethyl ether to remove adsorbed HBr on their surface followed by drying under vacuum overnight. Subsequently, the dried crystals were dissolved in dimethylformamide (DMF) to obtain a 0.5 M solution. The solution was spin-coated on a quartz substrate at 2000 rpm for 60 s and then annealed at 75 °C for 5 min followed by 100 °C for 15 min.

UV/Vis and NMR measurements

UV/Vis spectra were recorded by using a Shimadzu spectrophotometer (UV3600) with a scanning resolution of 0.5 nm. Steady-state PL spectra were measured using a Fluorolog-3, (HORIBA Jobin Yvon) spectrofluorometer system. NMR spectra were recorded using an AV 400 MHz NMR spectrometer equipped with two RF channels, 5 mm z-gradient BBO probe and one BACS-60 automatic sample changer. The morphology of the samples was characterized by SEM (JEOL, JSM-7600F).

Time resolved photoluminescence (TRPL)

The excitation source at 340 nm, $50 \mu\text{J cm}^{-2}$ was generated by an optical parametric amplifier (Coherent OPerA Solo) pumped by Coherent Libra regenerative amplifier (50 fs, 1 kHz, 800 nm). TRPL was collected using an Optronis Optoscope streak camera system having resolution of ≈ 200 ps for the settings used in this experiment. All optical measurements were performed at room temperature in ambient conditions.

Low-temperature measurements

The thin-film samples on glass were mounted in vacuum into a liquid-nitrogen-cooled Linkam Stage (FTIR 600) that allows varying the operating temperatures from room temperature down to 77 K.

X-ray crystal structure determination

A colourless plate-like (CyBMA)PbBr₄ crystal (0.080 mm \times 0.100 mm \times 0.500 mm) was used for the X-ray crystallographic analysis using a Bruker D8 Advance spectrometer. The total exposure time was 43 min. The frames were integrated with the Bruker SAINT Software package using a narrow-frame algorithm. The integration of the data using an orthorhombic unit cell yielded a total of 9972 reflections to a maximum θ angle of 31.20° (0.69 Å resolution), of which 2705 were independent (average redundancy 3.687, completeness = 98.9%, $R_{\text{int}} = 11.67\%$, $R_{\text{sig}} = 11.00\%$) and 1719 (63.55%) were greater than $2\sigma(F^2)$ ($\sigma =$ scattering cross section, $F =$ scattering factor). The final cell constants are based upon the refinement of the XYZ-centroids of 2801 reflections above $20\sigma(I)$ ($I =$ intensity) with $5.396 < 2\theta < 61.66$. Data were corrected for absorption effects using the multi-scan method (SADABS). The ratio of minimum-to-maximum apparent transmission was 0.236. The cal-

culated minimum and maximum transmission coefficients (based on crystal size) were 0.0360 and 0.2990. The structure was solved and refined using the Bruker SHELXTL Software Package.

Acknowledgements

This research was supported by the National Research Foundation, Prime Minister's Office, Singapore, under its Competitive Research Programme (CRP Award No. NRF-CRP14-2014-03). T.C.S. also acknowledges the financial support from the Singapore Ministry of Education Academic Research Fund Tier 1 grants RG101/15 and RG173/16, and Tier 2 grants MOE2014-T2-1-044 and MOE2015-T2-2-015.

Conflict of interest

The authors declare no conflict of interest.

Keywords: hybrid perovskites \oplus photoluminescence \oplus self-trapped excitons \oplus solar cells \oplus white-light emission

- [1] a) P. P. Boix, K. Nonomura, N. Mathews, S. G. Mhaisalkar, *Mater. Today* **2014**, *17*, 16–23; b) P. Gao, M. Gratzel, M. K. Nazeeruddin, *Energy Environ. Sci.* **2014**, *7*, 2448–2463.
- [2] NREL, http://www.nrel.gov/ncpv/images/efficiency_chart.jpg.
- [3] Z. Cheng, J. Lin, *CrystEngComm* **2010**, *12*, 2646–2662.
- [4] a) K. Chondroudis, D. B. Mitzi, *Chem. Mater.* **1999**, *11*, 3028–3030; b) D. Liang, Y. Peng, Y. Fu, M. J. Shearer, J. Zhang, J. Zhai, Y. Zhang, R. J. Hamers, T. L. Andrew, S. Jin, *ACS Nano* **2016**, *10*, 6897–6904; c) M. Yuan, L. N. Quan, R. Comin, G. Walters, R. Sabatini, O. Voznyy, S. Hoogland, Y. Zhao, E. M. Beauregard, P. Kanjanaboos, Z. Lu, D. H. Kim, E. H. Sargent, *Nat. Nano* **2016**, *11*, 872–877; d) J. Song, J. Li, X. Li, L. Xu, Y. Dong, H. Zeng, *Adv. Mater.* **2015**, *27*, 7162–7167; e) G. Li, F. W. Rivarola, N. J. Davis, S. Bai, T. C. Jellicoe, F. de la Pena, S. Hou, C. Ducati, F. Gao, R. H. Friend, N. C. Greenham, Z. K. Tan, *Adv. Mater.* **2016**, *28*, 3528–3534.
- [5] G. Xing, N. Mathews, S. S. Lim, N. Yantara, X. Liu, D. Sabba, M. Grätzel, S. Mhaisalkar, T. C. Sum, *Nat. Mater.* **2014**, *13*, 476–480.
- [6] S. Ahmad, P. K. Kanaujia, H. J. Beeson, A. Abate, F. Deschler, D. Credgington, U. Steiner, G. V. Prakash, J. J. Baumberg, *ACS Appl. Mater. Interfaces* **2015**, *7*, 25227–25236.
- [7] a) M. D. Birowosuto, D. Cortecchia, W. Drozdowski, K. Blylew, W. Lachmanski, A. Bruno, C. Soci, *Sci. Rep.* **2016**, *6*, 37257; b) K. Shibuya, M. Koshimizu, Y. Takeoka, K. Asai, *Nuclear Instruments Methods Phys. Res. Sect. B* **2002**, *194*, 207–212.
- [8] S. Ye, F. Xiao, Y. X. Pan, Y. Y. Ma, Q. Y. Zhang, *Mater. Sci. Eng. R* **2010**, *71*, 1–34.
- [9] Y. Y. Li, C. K. Lin, G. L. Zheng, Z. Y. Cheng, H. You, W. D. Wang, J. Lin, *Chem. Mater.* **2006**, *18*, 3463–3469.
- [10] E. R. Dohner, E. T. Hoke, H. I. Karunadasa, *J. Am. Chem. Soc.* **2014**, *136*, 1718–1721.
- [11] E. R. Dohner, A. Jaffe, L. R. Bradshaw, H. I. Karunadasa, *J. Am. Chem. Soc.* **2014**, *136*, 13154–13157.
- [12] Z. Yuan, C. Zhou, Y. Tian, Y. Shu, J. Messier, J. C. Wang, L. J. van de Burgt, K. Kountouriotis, Y. Xin, E. Holt, K. Schanze, R. Clark, T. Siegrist, B. Ma, *Nat. Commun.* **2017**, *8*, 14051.
- [13] a) A. Yangui, D. Garrot, J. S. Lauret, A. Lussan, G. Bouchez, E. Deleporte, S. Pillet, E. E. Bendeif, M. Castro, S. Triki, Y. Abid, K. Boukheddaden, *J. Phys. Chem. C* **2015**, *119*, 23638–23647; b) D. Cortecchia, J. Yin, A. Bruno, S.-Z. A. Lo, G. G. Gurzadyan, S. Mhaisalkar, J.-L. Bredas, C. Soci, *J. Mater. Chem. C* **2017**, *5*, 2771–2780; c) T. Hu, M. D. Smith, E. R. Dohner, M.-J. Sher, X. Wu, M. T. Trinh, A. Fisher, J. Corbett, X. Y. Zhu, H. I. Karunadasa, A. M. Lindenberg, *J. Phys. Chem. Lett.* **2016**, *7*, 2258–2263; d) J. Yin, H. Li, D. Cortecchia, C. Soci, J.-L. Bredas, *ACS Energy Lett.* **2017**, *2*, 417–423.

- [14] D. Cortecchia, S. Neutzner, A. R. Srimath Kandada, E. Mosconi, D. Meggiolaro, F. De Angelis, C. Soci, A. Petrozza, *J. Am. Chem. Soc.* **2017**, *139*, 39–42.
- [15] S. Bhaumik, S. A. Veldhuis, Y. F. Ng, M. Li, S. K. Muduli, T. C. Sum, B. Damodaran, S. Mhaisalkar, N. Mathews, *Chem. Commun.* **2016**, *52*, 7118–7121.
- [16] T. M. Koh, V. Shanmugam, J. Schlipf, L. Oesinghaus, P. Müller-Buschbaum, N. Ramakrishnan, V. Swamy, N. Mathews, P. P. Boix, S. G. Mhaisalkar, *Adv. Mater.* **2016**, *28*, 3653–3661.
- [17] a) A. D. Wright, C. Verdi, R. L. Milot, G. E. Eperon, M. A. Pérez-Osorio, H. J. Snaith, F. Giustino, M. B. Johnston, L. M. Herz, *Nat. Commun.* **2016**, *7*, 11755; b) L. Raimondo, L. Silvestri, A. Borghesi, S. Tavazzi, *J. Phys. Chem. C* **2013**, *117*, 26248–26254.
- [18] a) M. Fox, *Optical Properties of Solids, 2nd ed.*, Oxford Press, New York **2010**; b) V. D'Innocenzo, G. Grancini, M. J. P. Alcocer, A. R. S. Kandada, S. D. Stranks, M. M. Lee, G. Lanzani, H. J. Snaith, A. Petrozza, *Nat. Commun.* **2014**, *5*, 3586; c) Y. P. Varshni, *Physica* **1967**, *34*, 149–154.
- [19] a) A. Matsui, N. Hitoshi, *J. Phys. Soc. Jpn.* **1980**, *49*, 657–663; b) N. F. Mott, A. M. Stoneham, *J. Phys. C* **1977**, *10*, 3391; c) R. T. Williams, K. S. Song, *J. Phys. Chem. Solids* **1990**, *51*, 679–716; d) I. Y. Fugol', *Adv. Phys.* **1978**, *27*, 1–87.
- [20] a) C. C. Stoumpos, C. D. Malliakas, M. G. Kanatzidis, *Inorg. Chem.* **2013**, *52*, 9019; b) M. D. Smith, A. Jaffe, E. R. Dohner, A. M. Lindenberg, H. I. Karunadasa, *Chem. Sci.* **2017**, *8*, 4497–4504.
- [21] a) D. Cortecchia, S. Neutzner, A. R. Srimath Kandada, E. Mosconi, D. Meggiolaro, F. De Angelis, C. Soci, A. Petrozza, *J. Am. Chem. Soc.* **2017**, *139*, 39–42; b) L. L. Mao, Y. L. Wu, C. C. Stoumpos, M. R. Wasielewski, M. G. Kanatzidis, *J. Am. Chem. Soc.* **2017**, *139*, 5210–5215.
- [22] a) Y. Toyozawa, *Progr. Theoretical Phys.* **1961**, *26*, 29–44; b) V. G. Plekhanov, *Progr. Mater. Sci.* **2004**, *49*, 787–886.
- [23] A. Y. Kobitski, K. S. Zhuravlev, H. P. Wagner, D. R. T. Zahn, *Phys. Rev. B* **2001**, *63*, 115423.
- [24] J. C. Vial, A. Bsiesy, F. Gaspard, R. Hérino, M. Ligeon, F. Muller, R. Romestain, R. M. Macfarlane, *Phys. Rev. B* **1992**, *45*, 14171–14176.

Manuscript received: July 7, 2017

Accepted manuscript online: July 28, 2017

Version of record online: August 24, 2017